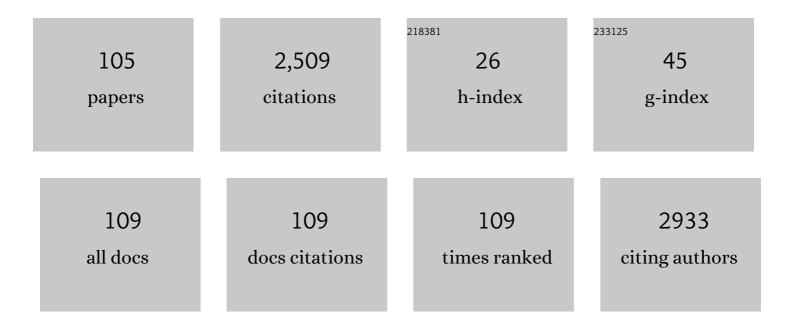
Klaus Achterhold

List of Publications by Year in descending order

Source: https://exaly.com/author-pdf/6570217/publications.pdf Version: 2024-02-01



#	Article	IF	CITATIONS
1	Development of a manufacturing process for Binder Jet 3D printed porous Al2O3 supports used in heterogeneous catalysis. Additive Manufacturing, 2022, 50, 102498.	1.7	6
2	Composition determination of kidney stones via wide angle X-ray scattering at an inverse Compton X-ray source. , 2022, , .		0
3	Experimental and numerical analysis of void structure in random packed beds of spheres. Powder Technology, 2021, 380, 613-628.	2.1	31
4	Heterogeneity of Graphite Lithiation in Stateâ€ofâ€theâ€Art Cylinderâ€Type Liâ€Ion Cells. Batteries and Supercaps, 2021, 4, 327-335.	2.4	8
5	Heterogeneity of Graphite Lithiation in Stateâ€ofâ€theâ€Art Cylinderâ€Type Liâ€Ion Cells. Batteries and Supercaps, 2021, 4, 251-251.	2.4	2
6	Laboratory-scale <i>in situ</i> X-ray absorption spectroscopy of a palladium catalyst on a compact inverse-Compton scattering X-ray beamline. Journal of Analytical Atomic Spectrometry, 2021, 36, 2649-2659.	1.6	4
7	Simultaneous two-color X-ray absorption spectroscopy using Laue crystals at an inverse-compton scattering X-ray facility. Journal of Synchrotron Radiation, 2021, 28, 1874-1880.	1.0	Ο
8	On the Mechanism of Catalytic Decarboxylation of Carboxylic Acids on Carbon-Supported Palladium Hydride. ACS Catalysis, 2021, 11, 14625-14634.	5.5	11
9	A proof of principle experiment for microbeam radiation therapy at the Munich compact light source. Radiation and Environmental Biophysics, 2020, 59, 111-120.	0.6	15
10	Dynamic K-edge Subtraction Fluoroscopy at a Compact Inverse-Compton Synchrotron X-ray Source. Scientific Reports, 2020, 10, 9612.	1.6	7
11	Biomedical x-ray imaging with a GaAs photon-counting detector: A comparative study. APL Photonics, 2020, 5, .	3.0	15
12	Technical and dosimetric realization of in vivo xâ€ray microbeam irradiations at the Munich Compact Light Source. Medical Physics, 2020, 47, 5183-5193.	1.6	3
13	Energy-Dispersive X-ray Absorption Spectroscopy with an Inverse Compton Source. Scientific Reports, 2020, 10, 8772.	1.6	26
14	Nanoscopic X-ray tomography for correlative microscopy of a small meiofaunal sea-cucumber. Scientific Reports, 2020, 10, 3960.	1.6	11
15	An approach to construct a three-dimensional isogeometric model from $\hat{1}$ /4-CT scan data with an application to the bridge of a violin. Computer Aided Geometric Design, 2020, 78, 101815.	0.5	3
16	Spectroscopic imaging at compact inverse Compton X-ray sources. Physica Medica, 2020, 79, 137-144.	0.4	6
17	The versatile X-ray beamline of the Munich Compact Light Source: design, instrumentation and applications. Journal of Synchrotron Radiation, 2020, 27, 1395-1414.	1.0	34
18	K-edge subtraction imaging for iodine and calcium separation at a compact synchrotron x-ray source. Journal of Medical Imaging, 2020, 7, 1.	0.8	6

KLAUS ACHTERHOLD

#	Article	IF	CITATIONS
19	The Versatile X-ray Beamline at the Munich Compact Light Source, an Inverse Compton Synchrotron Facility. , 2020, , .		0
20	Dose and spatial resolution analysis of grating-based phase-contrast mammography using an inverse Compton x-ray source. Journal of Medical Imaging, 2020, 7, 1.	0.8	0
21	Multimodal Precision Imaging of Pulmonary Nanoparticle Delivery in Mice: Dynamics of Application, Spatial Distribution, and Dosimetry. Small, 2019, 15, e1904112.	5.2	21
22	Contrast-enhanced spectral mammography with a compact synchrotron source. PLoS ONE, 2019, 14, e0222816.	1.1	11
23	3D Imaging of Soft-Tissue Samples using an X-ray Specific Staining Method and Nanoscopic Computed Tomography. Journal of Visualized Experiments, 2019, , .	0.2	2
24	K-edge Subtraction Computed Tomography with a Compact Synchrotron X-ray Source. Scientific Reports, 2019, 9, 13332.	1.6	16
25	X-ray imaging of a water bear offers a new look at tardigrade internal anatomy. Zoological Letters, 2019, 5, 14.	0.7	19
26	Visualizing treatment delivery and deposition in mouse lungs using in vivo x-ray imaging. Journal of Controlled Release, 2019, 307, 282-291.	4.8	27
27	Perfusion-ventilation CT via three-material differentiation in dual-layer CT: a feasibility study. Scientific Reports, 2019, 9, 5837.	1.6	8
28	Signal-to-thickness calibration and pixel-wise interpolation for beam-hardening artefact reduction in microCT. Europhysics Letters, 2019, 125, 38003.	0.7	3
29	A step towards valid detection and quantification of lung cancer volume in experimental mice with contrast agent-based X-ray microtomography. Scientific Reports, 2019, 9, 1325.	1.6	17
30	Device for source position stabilization and beam parameter monitoring at inverse Compton X-ray sources. Journal of Synchrotron Radiation, 2019, 26, 1546-1553.	1.0	11
31	In vivo x-ray imaging of the respiratory system using synchrotron sources and a compact light source. , 2019, , .		0
32	K-edge subtraction imaging for angiography at a compact synchrotron source. , 2019, , .		0
33	Dose and spatial resolution analysis of grating-based phase-contrast mammography using an inverse Compton x-ray source. , 2019, , .		0
34	Single-energy material decomposition with grating-based x-ray phase-contrast CT. , 2019, , .		0
35	Evaluation and optimization of multimodal x-ray imaging techniques for inverse Compton x-ray sources. , 2019, , .		0
36	New staining tools and developments for 3D soft tissue CT imaging. , 2019, , .		0

3

KLAUS ACHTERHOLD

#	Article	IF	CITATIONS
37	Three-dimensional virtual histology enabled through cytoplasm-specific X-ray stain for microscopic and nanoscopic computed tomography. Proceedings of the National Academy of Sciences of the United States of America, 2018, 115, 2293-2298.	3.3	85
38	Propagation-based phase-contrast x-ray tomography of cochlea using a compact synchrotron source. Scientific Reports, 2018, 8, 4922.	1.6	21
39	Tilted grating phase-contrast computed tomography using statistical iterative reconstruction. Scientific Reports, 2018, 8, 6608.	1.6	4
40	Laboratory-based X-ray NanoCT Explores Morphology of a Zebrafish Embryo. Microscopy and Microanalysis, 2018, 24, 184-185.	0.2	4
41	The Munich Compact Light Source: Flux Doubling and Source Position Stabilization At a Compact Inverse-Compton Synchrotron X-ray Source Microscopy and Microanalysis, 2018, 24, 316-317.	0.2	4
42	Nucleus-specific X-ray stain for 3D virtual histology. Scientific Reports, 2018, 8, 17855.	1.6	36
43	Dynamic X-ray Imaging at the Munich Compact Light Source. Microscopy and Microanalysis, 2018, 24, 352-353.	0.2	Ο
44	K-edge subtraction imaging for coronary angiography with a compact synchrotron X-ray source. PLoS ONE, 2018, 13, e0208446.	1.1	28
45	Direct quantitative material decomposition employing grating-based X-ray phase-contrast CT. Scientific Reports, 2018, 8, 16394.	1.6	30
46	X-ray dark-field imaging of the human lung—A feasibility study on a deceased body. PLoS ONE, 2018, 13, e0204565.	1.1	76
47	Dose-compatible grating-based phase-contrast mammography on mastectomy specimens using a compact synchrotron source. Scientific Reports, 2018, 8, 15700.	1.6	16
48	High resolution laboratory grating-based X-ray phase-contrast CT. Scientific Reports, 2018, 8, 15884.	1.6	25
49	CT scanning of membrane feed spacers – Impact of spacer model accuracy on hydrodynamic and solute transport modeling in membrane feed channels. Journal of Membrane Science, 2018, 564, 133-145.	4.1	21
50	In vivo Dynamic Phase-Contrast X-ray Imaging using a Compact Light Source. Scientific Reports, 2018, 8, 6788.	1.6	28
51	The Munich Compact Light Source: Biomedical Research At a Laboratory-Scale Inverse-Compton Synchrotron X-ray Source. Microscopy and Microanalysis, 2018, 24, 984-985.	0.2	4
52	The Munich Compact Light Source - Operating an Inverse Compton Source in User Mode. , 2018, , .		2
53	X-ray Beam Monitoring and Source Position Stabilization at an Inverse-Compton X-ray Source. , 2018, , .		1
54	Mono-Energy Coronary Angiography with a Compact Synchrotron Source. Scientific Reports, 2017, 7, 42211.	1.6	25

#	Article	IF	CITATIONS
55	Application of sensitive, highâ€resolution imaging at a commercial labâ€based Xâ€ray micro T system using propagationâ€based phase retrieval. Journal of Microscopy, 2017, 266, 211-220.	0.8	28
56	X-ray vector radiography of a human hand. , 2017, , .		2
57	Propagation-based Phase-Contrast X-ray Imaging at a Compact Light Source. Scientific Reports, 2017, 7, 4908.	1.6	38
58	Trabecular bone anisotropy imaging with a compact laser-undulator synchrotron x-ray source. Scientific Reports, 2017, 7, 14477.	1.6	26
59	Myoanatomy of the velvet worm leg revealed by laboratory-based nanofocus X-ray source tomography. Proceedings of the National Academy of Sciences of the United States of America, 2017, 114, 12378-12383.	3.3	52
60	In-vivo X-ray Dark-Field Chest Radiography of a Pig. Scientific Reports, 2017, 7, 4807.	1.6	83
61	Dual-energy micro-CT for quantifying the time-course and staining characteristics of ex-vivo animal organs treated with iodine- and gadolinium-based contrast agents. Scientific Reports, 2017, 7, 17387.	1.6	14
62	Increased cell survival and cytogenetic integrity by spatial dose redistribution at a compact synchrotron X-ray source. PLoS ONE, 2017, 12, e0186005.	1.1	12
63	Mono-energy coronary angiography with a compact light source. , 2017, , .		2
64	Obtaining the spacing factor of microporous concrete using high-resolution Dual Energy X-ray Micro CT. Cement and Concrete Research, 2016, 89, 200-205.	4.6	33
65	The Munich Compact Light Source: initial performance measures. Journal of Synchrotron Radiation, 2016, 23, 1137-1142.	1.0	131
66	Absorption and Phase Contrast X-Ray Imaging in Paleontology Using Laboratory and Synchrotron Sources. Microscopy and Microanalysis, 2015, 21, 1288-1295.	0.2	4
67	Optimization of propagation-based phase-contrast imaging at a laboratory setup. Optics Express, 2015, 23, 30000.	1.7	15
68	X-ray phase-contrast tomography with a compact laser-driven synchrotron source. Proceedings of the United States of America, 2015, 112, 5567-5572.	3.3	103
69	Optimization of propagation-based phase-contrast imaging at a laboratory setup. Optics Express, 2015, 23, 30000.	1.7	0
70	Applied x-ray computed tomography with high resolution in paleontology using laboratory and synchrotron sources. , 2014, , .		0
71	Energy-resolved visibility analysis of grating interferometers operated at polychromatic X-ray sources. Optics Express, 2014, 22, 30394.	1.7	25
72	A new sample environment for cryogenic nuclear resonance scattering experiments on single crystals and microsamples at P01, PETRA III. Hyperfine Interactions, 2014, 226, 673-678.	0.2	0

KLAUS ACHTERHOLD

#	Article	IF	CITATIONS
73	Helical differential X-ray phase-contrast computed tomography. Physica Medica, 2014, 30, 374-379.	0.4	19
74	An algebraic iterative reconstruction technique for differential X-ray phase-contrast computed tomography. Zeitschrift Fur Medizinische Physik, 2013, 23, 186-193.	0.6	25
75	Comparison of Contrast-to-Noise Ratios of Transmission and Dark-Field Signal in Grating-Based X-ray Imaging for Healthy Murine Lung Tissue. Zeitschrift Fur Medizinische Physik, 2013, 23, 236-242.	0.6	24
76	Translation of Atherosclerotic Plaque Phase-Contrast CT Imaging from Synchrotron Radiation to a Conventional Lab-Based X-Ray Source. PLoS ONE, 2013, 8, e73513.	1.1	25
77	Diagnosing and Mapping Pulmonary Emphysema on X-Ray Projection Images: Incremental Value of Grating-Based X-Ray Dark-Field Imaging. PLoS ONE, 2013, 8, e59526.	1.1	44
78	Experimental validation of image contrast correlation between ultra-small-angle X-ray scattering and grating-based dark-field imaging using a laser-driven compact X-ray source. Photonics & Lasers in Medicine, 2012, 1, .	0.3	19
79	Vibrational properties of the polymeric spin crossover (SCO) Fe(ii) complexes [{Fe(4-amino-1,2,4-triazole)3}X2]n: a nuclear inelastic scattering (NIS), Raman and DFT study. Physical Chemistry Chemical Physics, 2012, 14, 14650.	1.3	23
80	Emphysema diagnosis using X-ray dark-field imaging at a laser-driven compact synchrotron light source. Proceedings of the National Academy of Sciences of the United States of America, 2012, 109, 17880-17885.	3.3	167
81	Nuclear inelastic scattering of 1D polymeric Fe(II) complexes of 1,2,4-aminotriazole in their high-spin and low-spin state. Hyperfine Interactions, 2012, 204, 129-132.	0.2	12
82	Multimodal hard X-ray imaging of a mammography phantom at a compact synchrotron light source. Journal of Synchrotron Radiation, 2012, 19, 525-529.	1.0	33
83	Complete Twoâ€Step Spinâ€Transition in a 1D Chain Iron(II) Complex with a 110â€K Wide Intermediate Plateau. European Journal of Inorganic Chemistry, 2011, 2011, 3183-3192.	1.0	34
84	Dynamical properties of the hydration shell of fully deuterated myoglobin. Physical Review E, 2011, 84, 041930.	0.8	9
85	Vibrational properties of the trinuclear spin crossover complex [Fe3(4-(2′-hydroxy-ethyl)-1,2,4-triazole)6(H2O)6](CF3SO3)6: a nuclear inelastic scattering, IR, Raman and DFT study. Physical Chemistry Chemical Physics, 2010, 12, 14782.	1.3	27
86	Protein dynamics of a \hat{I}^2 -sheet protein. European Biophysics Journal, 2009, 38, 687-700.	1.2	12
87	Conformational changes in hemoglobin triggered by changing the iron charge. Hyperfine Interactions, 2008, 185, 103-110.	0.2	1
88	Synthesis and Characterisation of Two New Iron(II) Spin-Crossover Complexes with N4O2Coordination Spheres - Optimizing Preconditions for Cooperative Interactions. European Journal of Inorganic Chemistry, 2008, 2008, 4891-4898.	1.0	26
89	Cooperative Iron(II) Spin Crossover Complexes with N ₄ O ₂ Coordination Sphere. Inorganic Chemistry, 2008, 47, 487-496.	1.9	81
90	Synthesis and Characterization of a Dinuclear Iron(II) Spin Crossover Complex with Wide Hysteresis. Inorganic Chemistry, 2008, 47, 10779-10787.	1.9	62

#	Article	IF	CITATIONS
91	A Physical Picture of Protein Dynamics and Conformational Changes. Journal of Biological Physics, 2007, 33, 371-387.	0.7	20
92	Seeded Growth of Asymmetric Binary Nanocrystals Made of a Semiconductor TiO2Rodlike Section and a Magnetic Î ³ -Fe2O3Spherical Domain. Journal of the American Chemical Society, 2006, 128, 16953-16970.	6.6	163
93	Protein dynamics on different timescales. Journal of Non-Crystalline Solids, 2006, 352, 4371-4378.	1.5	12
94	Colloidal Synthesis and Characterization of Tetrapod-Shaped Magnetic Nanocrystals. Nano Letters, 2006, 6, 1966-1972.	4.5	140
95	Protein dynamics on different timescales. Journal of Physics and Chemistry of Solids, 2005, 66, 2257-2262.	1.9	21
96	Protein dynamics: determination of anisotropic vibrations at the haem iron of myoglobin. Journal of Physics Condensed Matter, 2003, 15, S1683-S1692.	0.7	25
97	Title is missing!. Hyperfine Interactions, 2002, 144/145, 209-222.	0.2	6
98	The X-ray absorption spectroscopy Debye-Waller factors of an iron compound and of met-myoglobin as a function of temperature. European Biophysics Journal, 2001, 30, 393-403.	1.2	16
99	Identification of Key Residues in Rabbit Liver Microsomal Cytochrome P450 2B4: Importance in Interactions with NADPH-Cytochrome P450 Reductase. Journal of Biochemistry, 2000, 127, 163-169.	0.9	22
100	Nuclear forward scattering of synchrotron radiation by deoxymyoglobin. European Biophysics Journal, 2000, 29, 146-152.	1.2	17
101	Protein dynamics studied on myoglobin. , 1999, 123/124, 825-840.		23
102	Simultaneous interpretation of M¶ssbauer, EPR and 57Fe ENDOR spectra of the [Fe4S4] cluster in the high-potential iron protein I Ectothiorhodospira halophila. Journal of Biological Inorganic Chemistry, 1999, 4, 727-741.	1.1	20
103	Determination of the phonon spectrum of iron in myoglobin using inelastic X-ray scattering of synchrotron radiation. European Biophysics Journal, 1997, 25, 221-224.	1.2	52
104	Temperature dependent inelastic X-ray scattering of synchrotron radiation on myoglobin analyzed by the Mössbauer effect. European Biophysics Journal, 1996, 25, 43-46.	1.2	21
105	Rayleigh scattering of Mössbauer radiation on a myoglobin single crystal. Hyperfine Interactions, 1992, 71, 1319-1322.	0.2	6